ChemPubSoc Europe

DOI: 10.1002/celc.201901781

CHEMELECTROCHEM Communications

Special Collection

Lowering Interfacial Dissolved Gas Concentration for Highly Efficient Hydrazine Oxidation at Platinum by Fluorosurfactant Modulation

Xu Zhao[+], Ruchiranga Ranaweera[+], Jason C. Mixdorf, Hien M. Nguyen,* and Long Luo*[a]

Regulating the dissolved-gas concentration at the electrode-solution interface represents a promising universal strategy to achieve high efficiency towards gas evolution reactions. Here, we present a facile method to modulate the interfacial dissolved-gas concentration using cationic fluorinated pyridinium sulfonate (CFPS) for highly efficient hydrazine oxidation (HzOR). We found that the interfacial dissolved-nitrogen concentration was effectively lowered by the cationic surfactant CFPS, while CFPS still ensured a sufficient exposure of the active sites during the HzOR. As a result, relative to pure Pt, the CFPS-modulated Pt exhibited a 2.1-fold higher current density and a lower overpotential for HzOR. This work presents a new avenue to achieve highly efficient hydrazine oxidation through regulating the interfacial gas concentration.

Hydrazine oxidation reaction (HzOR) plays a pivotal role in sustainable energy conversion systems. Direct hydrazine fuel cell (DHFC) has a high theoretical cell voltage of 1.56 V, which is higher than that of hydrogen (1.23 V), methanol (1.18 V), and formic acid (1.45 V) fuel cells.[1–4] However, the practical open-circuit voltage of DHFC is still much lower than the theoretical value, mainly due to the large activation barrier of the HzOR.[5] To improve HzOR efficiency, extensive studies have been performed. One most common strategy is to synthesize catalysts with a reactive lattice structure, facet, or morphology, which often involves the use of surfactants as the capping agent.[6–13] For example, benzyl mercaptan was applied to synthesize highly dispersed Ag nanoparticles with high HzOR activity.[14]

Besides controlling the catalyst structure during synthesis, surfactants can also regulate the gas bubble behavior to affect the efficiency of an electrocatalytic reaction.[15] In our previous work,[16] we have discovered that perfluorooctanesulfonate (PFOS), an anionic perfluorinated surfactant, effectively lowers the dissolved-H_2 concentration at the Pt electrode-solution interface during the hydrogen evolution reaction (HER) by promoting H_2 bubble nucleation and formation. Meanwhile, due to the electrostatic repulsion between PFOS and the negatively charged Pt surface during the HER, sufficient exposure of the electrode surface active area is realized. The reduced interfacial dissolved-H_2 concentration and sufficient surface exposure together lead to a remarkably enlarged hydrogen evolution current.

Guided by this previous work, we have developed a new facile cationic fluorosurfactant-modulation strategy to achieve enhanced HzOR activity. We synthesized a fluorinated pyridinium sulfonate surfactant (CFPS). Owing to the high surface activity of CFPS, the activation energy for N_2 bubble nucleation is reduced, leading to a decreased dissolved-gas concentration at the HzOR interface. The positive charge of CFPS also ensures the effective exposure of active sites during hydrazine oxidation. Benefited from both effects, the CFPS-modulated Pt showed a boosted catalytic activity towards HzOR. The CFPS-modulated Pt exhibited a current density of 10 mA cm^{-2} at 562 mV vs RHE, which was 2.1 times higher than that of pure Pt under the same potential.

First of all, fluorinated pyridinium sulfonate surfactant was synthesized following a previously reported method using fluoroalkyl ethylene iodide as the precursor (Scheme S1).[17] Briefly, 2-perfluorooctyl ethyl iodide was firstly heated with pyridine at 80 °C for 24 h to generate fluorinated pyridinium iodide (Scheme S2). The obtained product was confirmed by the ^{1}H NMR and ^{19}F NMR spectra with the existence of perfluorinated alkyl, methylene, and pyridinium groups (Figures S1 and S2). The as-prepared pyridinium iodide was then dissolved in methanol and treated with *p*-toluenesulfonic acid at 60 °C for 80 h to yield the final fluorinated pyridinium sulfonate (Scheme S3). Figures S3 and S4 show the ^{1}H NMR and ^{19}F NMR spectra of the final product, where the signals of the perfluorinated alkyl chain, methylene, methyl, pyridinium, and phenyl were observed, indicating the successful synthesis of cationic fluorinated pyridinium surfactant.

After synthesizing CFPS, we measured the surface tension of the HzOR solutions (0.5 M H_2SO_4 and 1 M N_2H_4) with different concentrations of CFPS to evaluate the surface activity of CFPS. As shown in Figure S5, the surface tension of the HzOR solution with 1×10^{-5} mg/mL of CFPS was measured to be 71 mN/m, which was lower than that of the surfactant-free solution. The surface tension decreases with the increasing CFPS concentration in the HzOR solution. The lowered surface tension in the presence of CFPS further confirms the successful preparation of the cationic fluorinated surfactant.

[a] X. Zhao,[+] R. Ranaweera,[+] J. C. Mixdorf, Prof. H. M. Nguyen, Prof. L. Luo
Department of Chemistry, Wayne State University,
Detroit, Michigan 48202, United States
E-mail: long.luo@wayne.edu
hien.nguyen@chem.wayne.edu

[+] These authors contributed equally to this work.

Supporting information for this article is available on the WWW under https://doi.org/10.1002/celc.201901781

Special Collection An invited contribution to the Richard M. Crooks Festschrift

© 2020 Wiley-VCH Verlag GmbH & Co. KGaA, Weinheim

To investigate the impact of modulated surface tension on the dissolved-gas concentration at HzOR interface, we fabricated Pt nanoelectrodes following a previously published method.[18–20] First, a Pt tip with a nanometer-sized sharp end was fabricated in $CaCl_2$ solution through applying a sinusoidal wave of 110 Hz frequency and 4.3 V amplitude. Figure S6 shows the representative scanning electron microscopy (SEM) images of a sharpened Pt tip. Then, the sharpened Pt tip was thermally sealed in a glass capillary. A Pt nanoelectrode was exposed after polishing the glass capillary, which was monitored by an electronic feedback circuit. The Pt nanoelectrode radius was estimated from the diffusion-limited current for proton reduction (Figure S7).[21] The Pt nanoelectrode was then employed to study the N_2 bubble nucleation from electrooxidation of hydrazine.

Figure 1A shows the cyclic voltammogram (CV) of a 19-nm-radius Pt nanoelectrode in a 0.5 M H_2SO_4 solution containing 1 M N_2H_4. As the potential was scanned positively, the anodic current increased in two steps until it reached a peak current value: the pre-wave region between 0 and 0.4 V and the exponential growth region after 0.4 V. This is because there are two major hydrazine species, hydrazinium $[N_2H_5]^+$ and hydrazinediium $[N_2H_6]^{2+}$, in the solution.[22,23] The *i-V* response was initially smooth and continuous, suggesting no bubble formation in this range.[24] Then the current suddenly dropped to a residual current value, corresponding to the generation of a single bubble that actively blocked the Pt nanoelectrode.[25] In the presence of 10^{-5} mg/mL CFPS, the peak current, i_p, for N_2 bubble nucleation at the CFPS-modulated Pt electrode (CFPS-Pt) was 4.0 nA, which is about half of that at pure Pt: 7.4 nA. Because of the proportional relationship between the peak current and the critical dissolved N_2 gas concentration (C_{N_2}) required for bubble nucleation as described by $i_p = 4nFD_{N_2}C_{N_2}a$, where n is the number of transferred electrons per N_2 molecule, D_{N_2} is the diffusivity of N_2, and a is the radius of the Pt electrode,[26–28] the significantly decreased peak current for CFPS-Pt indicates the efficiently lowered critical dissolved-N_2 concentration for bubble formation at the reaction interface. The C_{N_2} for CFPS-Pt with different CFPS concentrations are summarized in Figure 1B. Notably, the critical dissolved-N_2 concentration for CFPS-Pt at a concentration of 10^{-5} mg/mL was as low as 0.07 M relative to that of 0.13 M for pure Pt. Moreover, with the addition of fluorinated surfactant from 10^{-7} mg/mL to 10^{-5} mg/mL, the C_{N_2} for CFPS-Pt showed a decreasing trend, further demonstrating the modulated dissolved N_2 gas concentration at the reaction interface.

We further investigated the N_2 gas bubble behavior during HzOR in the presence of CFPS at the macroscopic level. We carried out HzOR using a Pt wire electrode by stepping the HzOR current from 5×10^{-6} A to 5×10^{-4} A with a duration time of 10 s and 10-fold increase in current for each step. As shown in Figure 2A, at 10^{-5} mg/mL CFPS, the optical images show the formation of N_2 gas bubbles at 1×10^{-5} A. In comparison, no bubble formation was observed at pure Pt until the applied current reached as high as 1×10^{-4} A (Figure 2B). The lowered current of CFPS-Pt for bubble formation is consistent with the reduced critical dissolved-N_2 concentration at the reaction interface for bubble nucleation in Figure 1.

As discussed above, the presence of CFPS limits the concentration of dissolved-N_2 at the electrode-solution interface by facilitating bubble nucleation and formation. Because the dissolved-gas concentration (C_g) and the concentration overpotential of a gas evolution reaction (η_c) are related by $\eta_c = s_g\frac{RT}{nF}\ln\frac{C_g}{C_g^{sat}}$, where s_g is the stoichiometric gas coefficient, n is the number of electrons participating in the reaction ($n=4$), C_g^{sat} is the saturation concentration of dissolved gas,[29–31] the CFPS-induced C_g decrease is expected to lead to a smaller η_c and higher electrocatalytic performance towards HzOR.

To evaluate the catalytic performance of CFPS-Pt for HzOR, we carried out electrochemical measurements using a standard three-electrode system. Figure 3A shows the CVs of CFPS-Pt and pure Pt in an N_2-saturated 0.5 M H_2SO_4 solution containing 10 mM N_2H_4 at a sweep rate of 50 mV/s. The current values were normalized using the electrochemical active surface area (ECSA) of Pt. The ECSA was estimated from the total charge in the hydrogen adsorption/desorption region of the cyclic voltammograms of CFPS-Pt and pure Pt in the corresponding H_2SO_4 solution (Figure S8).[32,33] Relative to pure Pt, the onset potential and peak potential of the CFPS-Pt with different CFPS concentrations (10^{-7}, 10^{-6}, and 10^{-5} mg/mL) all showed a negative shift, indicating the improved electrocatalytic HzOR activity. In particular, the peak current density for CFPS-Pt with a CFPS concentration of 10^{-5} mg/mL was 5.7 mA cm^{-2}, ~36% higher than that of 4.2 mA cm^{-2} for pure Pt. Figure 3B shows

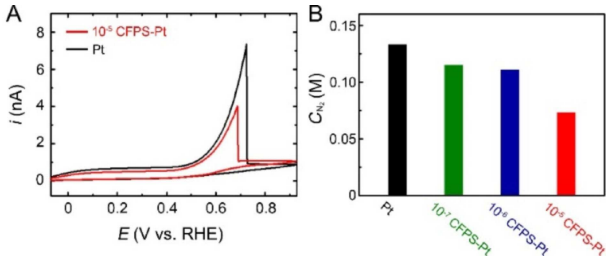

Figure 1. (A) Cyclic voltammograms of a 19-nm-radius Pt nanoelectrode in a 0.5 M H_2SO_4 solution containing 1 M N_2H_4 at a scan rate of 100 mV s^{-1} in the absence of CFPS and in the presence of 10^{-5} mg/mL CFPS. (B) Critical concentrations of dissolved N_2 gas required for bubble nucleation under different CFPS concentrations from 10^{-7} to 10^{-5} mg/mL.

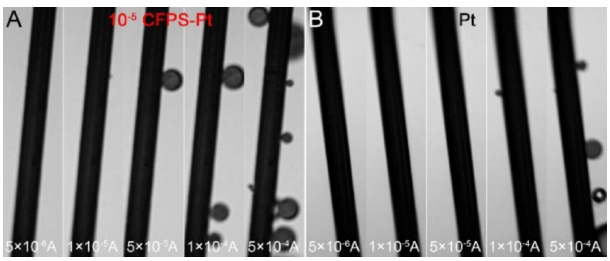

Figure 2. Micrographs of bubble generation on a Pt wire for (A) CFPS-Pt with 10^{-5} mg/mL CFPS and (B) pure Pt in a 0.5 M H_2SO_4 solution containing 10 mM N_2H_4. The anodic current passing the Pt wire was stepped from 5×10^{-6} A to 5×10^{-4} A to drive the HzOR.

© 2020 Wiley-VCH Verlag GmbH & Co. KGaA, Weinheim

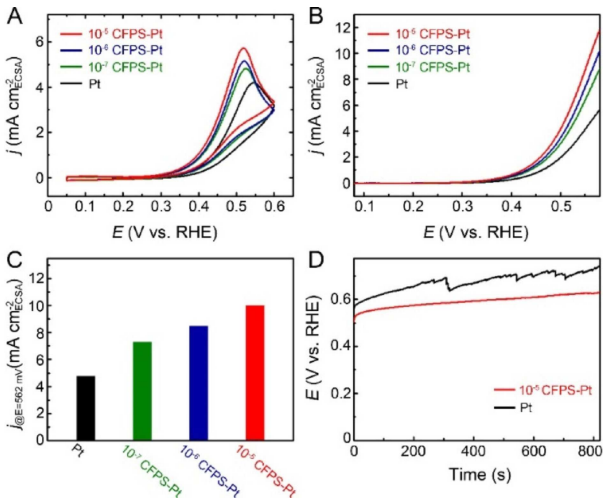

Figure 3. (A) Cyclic voltammograms and (B) *iR*-corrected polarization curves of CFPS-Pt with different CFPS concentrations (10^{-7}, 10^{-6}, and 10^{-5} mg/mL) and pure Pt recorded in N_2-saturated 0.5 M H_2SO_4 solution containing 10 mM N_2H_4. (C) Current densities of CFPS-Pt and pure Pt at the fixed potential of 562 mV vs RHE. (D) Galvanostatic measurements of CFPS-Pt and pure Pt at the HzOR current density of 10 mA cm^{-2}.

the polarization curves of CFPS-Pt and pure Pt recorded at a slow scan rate of 5 mV s^{-1} with a rotation speed of 900 rpm. The ohmic potential drop (*iR*) loss was corrected before comparison. We found all the CFPS-Pt exhibited a higher current density than pure Pt. The current densities for CFPS-Pt and pure Pt at a fixed potential of 562 mV vs RHE were summarized in Figure 3C. The CFPS-Pt with a CFPS concentration of 10^{-5} mg/mL showed the highest current density of 10 mA cm^{-2}, which is 2.1 times higher than that of pure Pt. We also conducted the galvanostatic measurements with prolonged reaction time in the same HzOR solution at a constant current density of 10 mA cm^{-2}. Figure 3D shows the potential for CFPS-Pt was consistently more negative than that for pure Pt. We have also tested 1 M N_2H_4 in 0.5 M H_2SO_4 solution and found a similar improvement in catalytic performance (Figure S9). All these results have shown the elevated HzOR activity with the modulation of CFPS.

Also, we have investigated the ECSA change of CFPS-Pt during the galvanostatic test to evaluate the interaction between CFPS and Pt surface during HzOR, which is believed to contribute to the improved HzOR performance of CFPS-Pt as well. We measured the ECSAs of CFPS-Pt and pure Pt before the galvanostatic test, and after 600 s and 1500 s of the test by taking out the electrode, immersing it in an N_2H_4-free 0.5 M H_2SO_4 solution, and collecting the charge in the H adsorption/desorption region (Figure S10). As shown in Figure S11, CFPS-Pt exhibited a slight ECSA loss of 0.6% after galvanostatic tests for 600 s, whereas the pure Pt showed a loss of 3.5%. After galvanostatic tests for 1500 s, the ECSA for CFPS-Pt dropped by 11.6%, whereas a substantial loss of 16.5% in ECSA was observed for pure Pt. This result shows CFPS did not cause any significant loss of active surface area-instead, it slowed down the surface deactivation, which should be a result of the electrostatic repulsion between CFPS and positively charged Pt surface during HzOR.[16,34] These results indicate the effective exposure of active sites during hydrazine oxidation with the modulation of CFPS.

To further understand the effect of CFPS on HzOR, we tested several other surfactants including PFOS, cetrimonium chloride (CTAC), sodium dodecyl sulfate (SDS), and Triton X-100 (TX100) for HzOR. Different surfactant concentrations were intentionally chosen so that all the surfactant-containing HzOR solutions exhibit a similar surface tension (Figure 4A). Figure 4B shows the corresponding bubble nucleation CV measured using a 15.3-nm-radius Pt nanoelectrode. Compared to pure Pt, the PFOS-, CTAC-, SDS-, and CFPS-modulated Pt all showed a smaller peak current for bubble nucleation, indicating these four surfactants can promote the bubble nucleation and lower the dissolved-N_2 concentration. Among them, CFPS showed the most significant impact on the bubble nucleation. The addition of TX100, however, did not alter the peak current, suggesting its incapability of modulating bubble nucleation and reducing the dissolved-gas concentration at the interface. The HzOR activity of these surfactants modulated Pt was evaluated and normalized to the measured ECSAs (Figure S12), respectively. Figures 4C and D show the polarization curves and the current densities at 562 mV vs RHE, respectively. The HzOR activity order is TX100-Pt, pure Pt < CTAC-Pt, PFOS-Pt < SDS-Pt < CFPS-Pt, in good agreement with the trend of their ability to promote bubble nucleation. This agreement confirms our theory that CFPS improves the HzOR performance of Pt by promoting bubble nucleation and lowering interfacial dissolved gas concentration. The reason for the slightly higher HzOR activity of SDS-Pt than that of CTAC- and PFOS-Pt, although they have very similar bubble nucleation current, is still unclear.

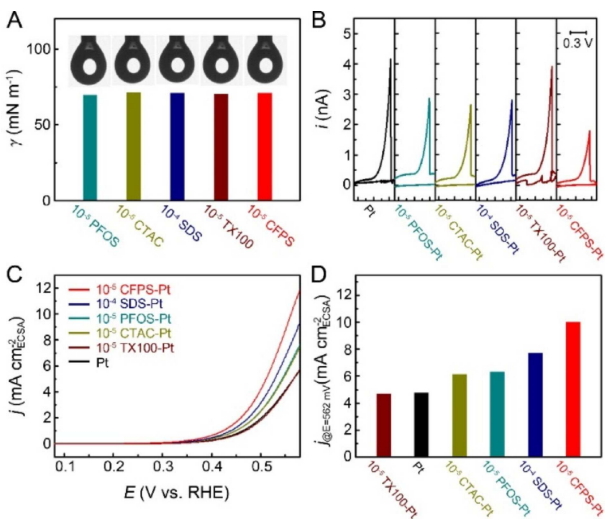

Figure 4. (A) Surface tension of surfactant-containing HzOR solutions (0.5 M H_2SO_4 and 1.0 M N_2H_4) measured by the pendant drop method. The surfactant concentrations are 10^{-5} mg/mL for PFOS, CTAC, TX100, and CFPS, and 10^{-4} mg/mL for SDS. (B) Cyclic voltammograms of a 15.3-nm-radius Pt nanoelectrode in these HzOR solutions at a scan rate of 100 mV s^{-1}. (C) *iR*-corrected polarization curves recorded at a scan rate of 5 mV s^{-1} and a rotation rate of 900 rpm in N_2-saturated 0.5 M H_2SO_4 solution containing 10 mM N_2H_4. (D) Comparison of HzOR current densities for different surfactant-modulated Pt at a fixed potential of 562 mV vs RHE.

© 2020 Wiley-VCH Verlag GmbH & Co. KGaA, Weinheim

In summary, we have demonstrated the use of a cationic fluorinated surfactant, CFPS, to regulate the dissolved-N_2 gas concentration at the reaction interface for highly efficient hydrazine electrooxidation. During HzOR, CFPS not only lowers the dissolved-N_2 gas concentration at electrode-solution interface but also ensures sufficient exposure of active electrode area, thereby leading to the remarkable catalytic performance.

Acknowledgements

This work was supported by start-up funds, Ebbing Faculty Development Award, and University Research Grant from Wayne State University to L.L. Financial support from Wayne State University and Carl Johnson Endowed Chair for H.M.N. is gratefully acknowledged. J.C.M. thanks the Nuclear Regulatory Commission Program (NRC-HQ-84-14-G-0037) for the graduate fellowship at the University of Iowa.

Keywords: electrocatalytic interface · gas concentration · cationic fluorosurfactant · hydrazine oxidation reaction

[1] T. Z. Wang, Q. Wang, Y. C. Wang, Y. L. Da, W. Zhou, Y. Shao, D. B. Li, S. H. Zhan, J. Y. Yuan, H. Wang, *Angew. Chem. Int. Ed.* **2019**, *58*, 13466; *Angew. Chem.* **2019**, *131*, 13600.
[2] Y. Y. Meng, X. X. Zou, X. X. Huang, A. Goswami, Z. W. Liu, T. Asefa, *Adv. Mater.* **2014**, *26*, 6510.
[3] K. Ojha, E. M. Farber, T. Y. Burshtein, D. Eisenberg, *Angew. Chem. Int. Ed.* **2018**, *57*, 17168; *Angew. Chem.* **2018**, *130*, 17414.
[4] H.-S. Lee, J.-K. Yu, J.-Y. Kim, K.-H. Kim, Y.-W. Rhee, *Stud. Surf. Sci. Catal.* **2006**, *159*, 589.
[5] T. Zhang, T. Asefa, *Adv. Mater.* **2019**, *31*, 1804394.
[6] J. Qian, M. Shen, S. Zhou, C.-T. Lee, M. Zhao, Z. H. Lyu, Z. D. Hood, M. Vara, K. D. Gilroy, K. Wang, Y. N. Xia, *Mater. Today* **2018**, *21*, 834.
[7] D. Huo, M. J. Kim, Z. H. Lyu, Y. F. Shi, B. J. Wiley, Y. N. Xia, *Chem. Rev.* **2019**, *119*, 8972.
[8] Z. C. Fang, Y. C. Wang, C. X. Liu, S. Chen, W. Sang, C. Wang, J. Zeng, *Small.* **2015**, *11*, 2593.
[9] H. W. Huang, H. H. Jia, Z. Liu, P. F. Gao, J. T. Zhao, Z. L. Luo, J. L. Yang, J. Zeng, *Angew. Chem. Int. Ed.* **2017**, *56*, 3594; *Angew. Chem.* **2017**, *129*, 3648.
[10] Z. M. Peng, H. Yang, *Nano Today* **2009**, *4*, 143.
[11] X. Zhao, S. Chen, Z. C. Fang, J. Ding, W. Sang, Y. C. Wang, J. Zhao, Z. M. Peng, J. Zeng, *J. Am. Chem. Soc.* **2015**, *137*, 2804.
[12] Q. Li, S. H. Sun, *Nano Energy* **2016**, *29*, 178.
[13] J. Feng, C. B. Gao, Y. D. Yin, *Nanoscale* **2018**, *10*, 20492.
[14] G. W. Yang, G. Y. Gao, C. Wang, C. L. Xu, H. L. Li, *Carbon* **2008**, *46*, 747.
[15] X. Zhao, H. Ren, L. Luo, *Langmuir* **2019**, *35*, 5392.
[16] X. Zhao, R. Ranaweera, L. Luo, *Chem. Commun.* **2019**, *55*, 1378.
[17] A. Yake, T. Corder, K. Moloy, T. Coope, C. Taylor, M. Huang, S. Peng, *J. Fluorine Chem.* **2016**, *187*, 46.
[18] B. Zhang, J. Galusha, P. G. Shiozawa, G. L. Wang, A. J. Bergren, R. M. Jones, R. J. White, E. N. Ervin, C. C. Cauley, H. S. White, *Anal. Chem.* **2007**, *79*, 4778.
[19] Q. J. Chen, R. Ranaweera, L. Luo, *J. Phys. Chem. C* **2018**, *122*, 15421.
[20] Y. W. Liu, M. A. Edwards, S. R. German, Q. J. Chen, H. S. White, *Langmuir* **2017**, *33*, 1845.
[21] R. Ranaweera, C. Ghafari, L. Luo, *Anal. Chem.* **2019**, *91*, 7744.
[22] J.-P. Schirmann, P. Bourdauducq, *Ullmann's Encyclopedia of Industrial Chemistry*, *Wiley-VCH*, *Weinheim*, **2002**, doi:10.1002/14356007.a13_177.
[23] T. M. Klapotke, P. S. White, I. C. Tornieporth-Oetting, *Polyhedron* **1996**, *15*, 2579.
[24] L. Luo, H. S. White, *Langmuir* **2013**, *29*, 11169.
[25] S. R. German, M. A. Edwards, H. Ren, H. S. White, *J. Am. Chem. Soc.* **2018**, *140*, 4047.
[26] Q. J. Chen, H. S. Wiedenroth, S. R. German, H. S. White, *J. Am. Chem. Soc.* **2015**, *137*, 12064.
[27] H. Ren, S. R. German, M. A. Edwards, Q. J. Chen, H. S. White, *J. Phys. Chem. Lett.* **2017**, *8*, 2450.
[28] S. R. German, M. A. Edwards, Q. J. Chen, Y. W. Liu, L. Luo, H. S. White, *Faraday Discuss.* **2016**, *193*, 223.
[29] J. Dukovic, C. W. Tobias, *J. Electrochem. Soc.* **1987**, *134*, 331.
[30] C. Gabrielli, F. Huet, R. P. Nogueira, *Electrochim. Acta* **2005**, *50*, 3726.
[31] H. Vogt, *J. Electrochem. Soc.* **1990**, *137*, 1179.
[32] B. Lim, M. J. Jiang, P. H. C. Camargo, E. C. Cho, J. Tao, X. M. Lu, Y. M. Zhu, Y. N. Xia, *Science* **2009**, *324*, 1302.
[33] A. Guha, T. V. Vineesh, A. Sekar, S. Narayanaru, M. Sahoo, S. Nayak, S. Chakraborty, T. N. Narayanan, *ACS Catal.* **2018**, *8*, 6636.
[34] N. Liu, Q. D. Zhang, R. X. Qu, W. F. Zhang, H. F. Li, Y. Wei, L. Feng, *Langmuir* **2017**, *33*, 7380.

Manuscript received: October 22, 2019
Revised manuscript received: November 13, 2019
Accepted manuscript online: November 14, 2019

© 2020 Wiley-VCH Verlag GmbH & Co. KGaA, Weinheim